


 Cite this: *Chem. Commun.*, 2016, 52, 2752

 Received 18th September 2015,  
 Accepted 4th January 2016

DOI: 10.1039/c5cc07818k

www.rsc.org/chemcomm

# Multifunctional organic nanoparticles with aggregation-induced emission (AIE) characteristics for targeted photodynamic therapy and RNA interference therapy†

 Guorui Jin,<sup>‡a</sup> Guangxue Feng,<sup>b</sup> Wei Qin,<sup>c</sup> Ben Zhong Tang,<sup>cd</sup> Bin Liu<sup>\*ab</sup> and Kai Li<sup>§\*a</sup>

**We report the design of AIE fluorogen (AIEGen)-based multifunctional organic nanoparticles with surface siRNA decoration for targeted photodynamic therapy and RNA interference therapy.**

Nanoparticle-based theranostic platforms that allow the incorporation of both imaging and therapeutic reagents into one single probe are strongly desired for cancer diagnosis and treatment, which facilitate concurrent image-guided diagnosis and therapies.<sup>1</sup> Among the various theranostic platforms, photodynamic therapy (PDT) has been increasingly recognized as an attractive approach for cancer treatment because the PDT treatment regulated by a beam of light has distinct advantages such as precise controllability, minimal invasive nature and high spatiotemporal accuracy.<sup>2</sup> The mechanism of PDT is that the photosensitizers are able to generate toxic reactive oxygen species (ROS) after light irradiation to kill tumor cells. Additionally, the fluorescence from photosensitizers could also facilitate the imaging-guided theranostic process. However, traditional fluorescent photosensitizers generally suffer from  $\pi$ - $\pi$  stacking due to the intrinsic hydrophobic and rigid planar molecular structures, further leading to aggregation caused quenching (ACQ) and significant decrease in ROS generation.<sup>3</sup> Recently, we have demonstrated that a class of fluorogens with

aggregation-induced emission (AIEgens) characteristics could act as effective fluorescent materials for theranostic applications.<sup>4</sup> The propeller-shaped AIEgens are generally non-emissive in solution but become highly emissive upon aggregation caused by the restriction of intramolecular rotations, which block the non-radiative pathway and activate the radiative channels for energy dissipation.<sup>5</sup> As such, the AIEGen-based photosensitizers are excellent key components for PDT with the expectation to yield bright emission and high phototoxicity upon loading into nanocarriers.<sup>6</sup> This is in contrast to the traditional ACQ photosensitizers, which offer quenched fluorescence and reduced phototoxicity in the nanoparticle (NP) format.<sup>7</sup>

Another challenge in PDT is that the cancer cells could respond to ROS stress by upregulating the level of vascular endothelial growth factor (VEGF) to suppress cellular senescence by inducing angiogenesis.<sup>8</sup> As a result, the resistance process in tumors treated with PDT will attenuate its therapeutic effect. To address this issue, the small interfering RNA-vascular endothelial growth factor (siVEGF) that has been widely used to suppress VEGF expression for inhibition of tumor growth and metastasis in cancer treatments has been used to provide a promising solution.<sup>9</sup> However, the delivery of short small interfering RNA (siRNA) remains a key challenge in the development of RNA interference (RNAi) therapeutics because of the poor stability of siRNA in a biological environment.<sup>10</sup> Recently, it was found that the stability of siRNA against enzymatic degradation could be improved when siRNA conjugated poly(ethylene glycol)-lipid forms a nanocarrier.<sup>11</sup> Considering the above mentioned facts, a new multifunctional theranostic platform based on AIE photosensitizers with the ability for siRNA delivery will offer a synergistic effect to achieve improved therapeutic outcome in an image-guided PDT.

In this contribution, we report multifunctional organic NPs using an AIEGen, 2-(2,6-bis((*E*)-4-(phenyl(4'-(1,2,2-triphenylvinyl)-[1,1'-biphenyl]-4-yl)amino)styryl)-4*H*-pyran-4-ylidene)malononitrile (TTD), as the photosensitizer with the biocompatible poly(ethylene glycol)-lipid as the encapsulation matrix. The surface of NPs was decorated with the cyclic arginine-glycine-aspartic acid (cRGD) peptide and siVEGF, which equipped the NPs with the ability to

<sup>a</sup> Institute of Materials Research and Engineering, A\*STAR, 2 Fusionopolis Way, Innovis, #08-03, 138634, Singapore. E-mail: kai\_li\_cn@hotmail.com

<sup>b</sup> Department of Chemical and Biomolecular Engineering, National University of Singapore, 4 Engineering Drive 4, 117585, Singapore. E-mail: cheliub@nus.edu.sg

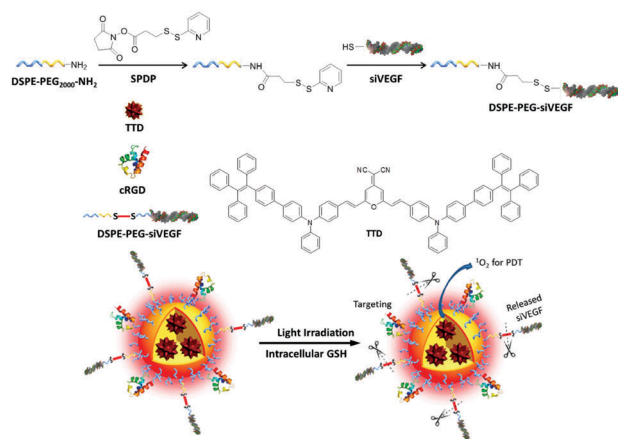
<sup>c</sup> Department of Chemistry, Institute for Advanced Study, Institute of Molecular Functional Materials, Division of Biomedical Engineering, Division of Life Science, and State Key Laboratory of Molecular Neuroscience, The Hong Kong University of Science & Technology, Clear Water Bay, Kowloon, Hong Kong, China

<sup>d</sup> Guangdong Innovative Research Team, SCUT-HKUST Joint Research Laboratory, State Key Laboratory of Luminescent Materials and Devices, South China University of Technology, Guangzhou, 510640, China

† Electronic supplementary information (ESI) available: Experimental part and additional data. See DOI: 10.1039/c5cc07818k

‡ Current address: The Key Laboratory of Biomedical Information Engineering of Ministry of Education, School of Life Science and Technology, Xi'an Jiaotong University, Xi'an, 710049, China.

§ Current address: Department of Radiology and Molecular Imaging Program at Stanford (MIPS), Stanford School of Medicine, Stanford, 94305, USA.



**Scheme 1** Illustration of conjugation of DSPE-PEG-NH<sub>2</sub> with siVEGF and formation of the TTD loaded and cRGD conjugated siVEGF-TTD nanoparticles (cRGD-siVEGF-TTD NPs). Succinimidyl 3-(2-pyridyldithio)propionate (SPDP) is the linker applied for conjugation of siVEGF with DSPE-PEG-NH<sub>2</sub>.

target integrin-overexpressed cells and deliver siRNA. By introducing the glutathione (GSH) cleavable disulfide bond between DSPE-PEG and siVEGF, the elevated GSH level in cell cytoplasm could release siVEGF from the NP surface. As a result, the internalized NPs could trigger a synergistic effect with combination of PDT and siRNA therapy to improve the overall killing efficiency towards MDA-MB-231 cells (Scheme 1). As compared to existing systems,<sup>12</sup> our “all-in-one” anti-cancer platform based on the AIE photosensitizer contains functionalities required for image, therapy, and RNA interference.<sup>13</sup>

The fluorescent photosensitizer TTD was synthesized according to our previous report.<sup>14</sup> DSPE-PEG-siVEGF was synthesized through the conjugation of DSPE-PEG-NH<sub>2</sub> with thiol-modified siVEGF using succinimidyl 3-(2-pyridyldithio)propionate (SPDP) as a linker.<sup>15</sup> Reverse-phase high performance liquid chromatography (HPLC) was applied to verify the success of conjugation. The HPLC peaks for DSPE-PEG-NH<sub>2</sub>, DSPE-PEG-siVEGF and siVEGF are observed at 6.985, 7.625 and 7.960 min retention time, respectively (Fig. S1, ESI<sup>†</sup>). The shift of the retention time of siVEGF from 7.960 min to 7.625 min indicates the successful conjugation of siVEGF with DSPE-PEG-NH<sub>2</sub>. The siVEGF-TTD NPs were then prepared by nanoprecipitation using a mixture of DSPE-PEG-siVEGF and DSPE-PEG-maleimide as the encapsulation matrix. The maleimide-decorated NPs were further immobilized with cRGD-SH, which facilitates the targeting ability to cancer cells with a high expression level of  $\alpha_v\beta_3$  integrin. The obtained cRGD-siVEGF-TTD NPs are spherical in shape under TEM (Fig. 1A) with an effective average hydrodynamic diameter of  $127 \pm 30$  nm determined by dynamic light scattering. The optical properties of cRGD-siVEGF-TTD NPs were also studied, which showed intense absorption peaks at 350 and 494 nm with an emission maximum at 682 nm in water (Fig. 1B). It has been reported that the TTD molecules showed typical twisted intramolecular charge transfer and AIE characteristics (Fig. S2, ESI<sup>†</sup>),<sup>14</sup> which yielded cRGD-siVEGF-TTD NPs with a quantum yield of  $(12\% \pm 1\%)$  in water (inset in Fig. 1B), measured using Rhodamine 6G in methanol as the standard.

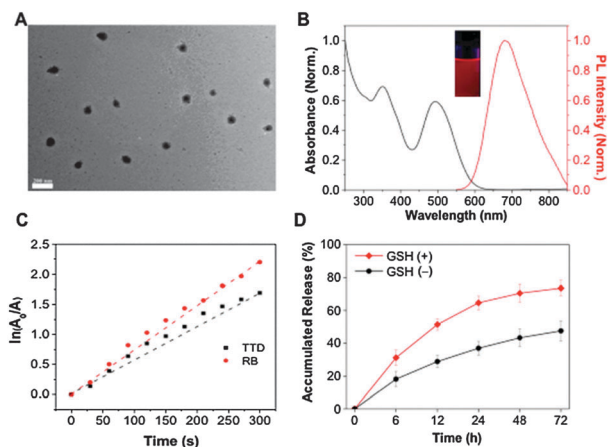


**Fig. 1** (A) Transmission electron microscopy (TEM) image of cRGD-siVEGF-TTD NPs. The scale bar is 200 nm. (B) UV-vis absorption and emission ( $\lambda_{\text{ex}} = 494$  nm) spectra of cRGD-siVEGF-TTD NPs in water. The inset shows a photo of NPs in water under UV lamp. (C) The decomposition rates of ABDA in the presence of cRGD-siVEGF-TTD NPs and RB;  $A_0$  and  $A$  are the absorbance of ABDA in the presence of the photosensitizers at 378 nm before and after irradiation, respectively. (D) Time course of release profiles of siVEGF from cRGD-siVEGF-TTD NPs in 1× PBS buffer with or without GSH at 37 °C.

Typically, intersystem crossing occurs from the singlet excited state to the triplet state upon excitation of the photosensitizers, which is followed by reaction with molecular oxygen to yield ROS, including singlet oxygen (<sup>1</sup>O<sub>2</sub>).<sup>16</sup> To achieve satisfied therapeutic outcome, photosensitizers with a high <sup>1</sup>O<sub>2</sub> yield is desirable.<sup>17</sup> Therefore, the <sup>1</sup>O<sub>2</sub> quantum yield of cRGD-siVEGF-TTD NPs ( $\Phi_{\text{TTD}}$ ) was quantified using 9,10-anthracenediyl-bis(methylene)dimalonic acid (ABDA) as the indicator and Rose Bengal (RB) as the standard photosensitizer (the <sup>1</sup>O<sub>2</sub> quantum yield for  $\Phi_{\text{RB}}$  is 75% in water).<sup>18</sup> In the presence of <sup>1</sup>O<sub>2</sub>, ABDA could undergo oxidation to yield endoperoxide, resulting in a decrease of ABDA absorption.<sup>19</sup> Under white light irradiation, the absorbance of ABDA solution with cRGD-siVEGF-TTD NPs decreased gradually with prolonged irradiation time (Fig. S3, ESI<sup>†</sup>), indicating the generation of <sup>1</sup>O<sub>2</sub> from cRGD-siVEGF-TTD NPs in the solution. The absorbance of ABDA in the presence of the photosensitizer (cRGD-siVEGF-TTD NPs or RB) at 378 nm before and after irradiation was defined as  $A_0$  and  $A$ , respectively. The plot of  $\ln(A_0/A)$  against time gives straight lines in Fig. 1C. From the slopes, the decomposition rate constants ( $K_{\text{TTD}}$ ) of cRGD-siVEGF-TTD NPs and RB ( $K_{\text{RB}}$ ) could be calculated as 0.0058 and 0.0072, respectively. The integrations of the optical absorption in the wavelength range of 400–800 nm for RB ( $A_{\text{RB}}$ ) and cRGD-siVEGF-TTD NPs ( $A_{\text{TTD}}$ ) were 21.09 and 18.68, respectively. The <sup>1</sup>O<sub>2</sub> quantum yield of cRGD-siVEGF-TTD NPs was calculated to be 68.2%. The *in vitro* release profiles of siVEGF from cRGD-siVEGF-TTD NPs were also studied in 1× PBS buffer with or without GSH. The concentration of GSH solution is 10 mM, mimicking intracellular reductive conditions.<sup>20</sup> It is known that the concentration of GSH in intracellular compartments is significantly higher than that in extracellular plasma and the difference in GSH concentration between cytoplasm and extracellular space provides a great potential in achieving highly efficient delivery and controlled release of siVEGF that was conjugated on the surface of

cRGD-siVEGF-TTD NPs through disulfide bonds.<sup>21</sup> As shown in Fig. 1D, faster release of siVEGF was triggered in the presence of GSH, suggesting that 31% and 73% of the siVEGF were released in the GSH-supplemented buffer after 6 and 72 h, respectively. However, only 18% and 47% of the siVEGF were released in buffer without GSH after 6 and 72 h, respectively. These data revealed that the effective intracellular release of siVEGF could be expected in cell cytoplasm upon internalization.

The targeting effect of cRGD-siVEGF-TTD NPs was investigated using MDA-MB-231 cancer cells with overexpressed  $\alpha_v\beta_3$  integrin as the target cells, while MCF-7 and SK-BR-3 cancer cells with low expression level of  $\alpha_v\beta_3$  integrin were used as the negative controls.<sup>22</sup> The fluorescence signals of NPs in MDA-MB-231, MCF-7 and SK-BR-3 cells were recorded under a confocal microscope after incubation with cRGD-siVEGF-TTD NPs at  $5 \mu\text{g mL}^{-1}$  of TTD for 4 h. As shown in Fig. 2, strong red fluorescence from the internalized NPs in the cytoplasm was clearly observed in MDA-MB-231 cells (Fig. 2A). In contrast, the MCF-7 and SK-BR-3 cells showed much weaker fluorescence, indicating the higher internalization efficiency of cRGD-functionalized NPs in MDA-MB-231 cells. This observation was consistent with the mean fluorescence intensity of each cell quantitatively analyzed by ImageJ from confocal images of MDA-MB-231, MCF-7, and SK-BR-3 cells (Fig. S4, ESI<sup>†</sup>). To evaluate the ROS productivity by cRGD-siVEGF-TTD NPs after cancer cell uptake, a cell permeable fluorescent reagent (CellROX<sup>®</sup> deep red reagent) was employed to detect the ROS generation under light irradiation. In the presence of ROS, the CellROX<sup>®</sup> deep red reagent could be rapidly oxidized to exhibit a strong red fluorescence. As shown in Fig. 2B, a strong red fluorescence was observed from the cell cytoplasm, suggesting efficient ROS generation from the cRGD-siVEGF-TTD NPs. The NP-treated cells without light irradiation were used as control. No fluorescence could be observed from the cells under a confocal microscope with the same parameters (Fig. S5, ESI<sup>†</sup>), further confirming that the red fluorescence is only from the oxidized CellROX<sup>®</sup> deep red reagent in the presence of ROS.

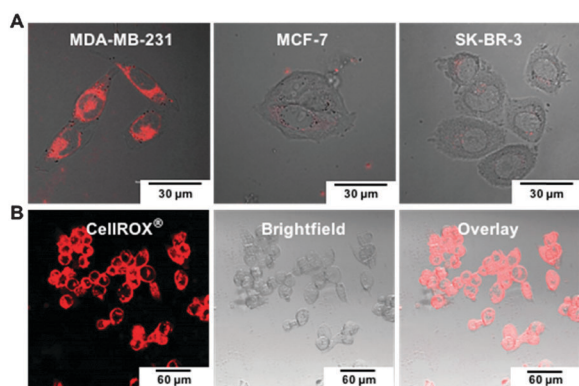


**Fig. 2** (A) Confocal images of MDA-MB-231, MCF-7, and SK-BR-3 cells after incubation with cRGD-siVEGF-TTD NPs ( $5 \mu\text{g mL}^{-1}$  of TTD) for 4 h at  $37^\circ\text{C}$ . The red fluorescence signal was from cRGD-siVEGF-TTD NPs ( $\lambda_{\text{ex}} = 488 \text{ nm}$  with a 560 nm above longpass filter). (B) Detection of intracellular ROS generation in living MDA-MB-231 cells after incubation with cRGD-siVEGF-TTD NPs ( $5 \mu\text{g mL}^{-1}$  of TTD) and CellROX<sup>®</sup> deep red reagent, followed by light irradiation ( $\lambda_{\text{ex}} = 633 \text{ nm}$ ; 650 nm above longpass filter).

Several research groups have reported that the overexpression of angiogenic factors (such as VEGF) in tumor cells after PDT could lead to the cell resistance to PDT.<sup>23</sup> To eliminate such resistance induced by angiogenesis following PDT, cRGD-siVEGF-TTD NPs with surface siVEGF conjugation were delivered to the targeted cancer cells, and confocal laser scanning microscopy (CLSM) was employed to visualize the cellular delivery of siVEGF. As cRGD-siVEGF-TTD NPs are red emissive, Cy3 modified siVEGF and cRGD were incorporated into a green AIEgen of 4,7-bis[4-(1,2,2-triphenylvinyl)phenyl]benzo-2,1,3-thiadiazole (BTPETD) based NPs fabricated using the same method as that used for red cRGD-siVEGF-TTD NPs. The obtained cRGD-Cy3-siVEGF-BTPETD NPs have an average size of  $\sim 130 \text{ nm}$ , and the green fluorescence could be effectively differentiated from the red signal for Cy3 conjugated siVEGF during confocal imaging (Fig. S6, ESI<sup>†</sup>). After incubation with MDA-MB-231 cells for 4 h, both green and red signals from BTPETD and Cy3 were detected from the cytoplasm with good coherence (Fig. S7, ESI<sup>†</sup>), suggesting that the siVEGF could be successfully delivered into target cells. The effect of siVEGF delivery on VEGF expression in target cells was further quantitatively evaluated through investigation of the relative VEGF protein and mRNA levels in MDA-MB-231 cells after incubation with cRGD-siVEGF-TTD NPs. After incubating the cells with cRGD-siVEGF-TTD NPs for 4 h, followed by culturing in fresh medium for another 48 h, VEGF protein in culture medium and VEGF mRNA in cell lysate were then individually analyzed using the VEGF Quantikine ELISA Kit and reverse transcription polymerase chain reaction (RT-PCR), respectively. As shown in Fig. 3A, cRGD-siVEGF-TTD NPs could effectively downregulate the VEGF protein expression level by 50% and the VEGF mRNA expression level by 64% as compared to the cells without NP treatment. As a result, the delivered siVEGF could significantly reduce VEGF expression, leading to attenuated resistance to PDT in cancer cells.<sup>24</sup>

To evaluate the cytotoxicity of TTD, cRGD-TTD NPs without siVEGF were fabricated from the same nanoprecipitation method using DSPE-PEG-Mal as the encapsulation matrix. MTT results indicated that the viability of MDA-MB-231 cells was kept at above 90% after incubation with cRGD-TTD NPs at 10, 20 and  $30 \mu\text{g mL}^{-1}$  of TTD for 48 h, indicating the low cytotoxicity of cRGD-TTD NPs to cells (Fig. S8, ESI<sup>†</sup>). The synergistic effect of PDT and RNAi therapy from cRGD-siRNA-TTD NPs was further evaluated by

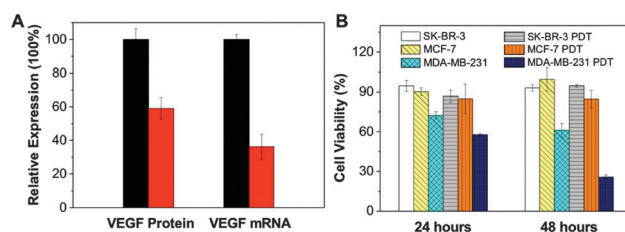


**Fig. 3** (A) The relative VEGF protein level in culture medium of cRGD-siVEGF-TTD NPs ( $5 \mu\text{g mL}^{-1}$  of TTD) treated MDA-MB-231 cells and the VEGF mRNA level determined from the lysate of MDA-MB-231 cells. Controls were shown in black and set to be 100%. (B) Viability of MDA-MB-231, MCF-7 and SK-BR-3 cells after incubation with cRGD-siVEGF-TTD NPs ( $5 \mu\text{g mL}^{-1}$  of TTD) for 4 h followed by light irradiation ( $0.20 \text{ W cm}^{-2}$ , 10 min) and further incubation in fresh medium for 24 and 48 h. Data present mean values  $\pm$  standard deviation,  $n = 3$ .

the MTT assay. SK-BR-3, MCF-7 and MDA-MB-231 cells were incubated with cRGD-siRNA-TTD NPs at  $5 \mu\text{g mL}^{-1}$  of TTD for 4 h. The free NPs were washed away and the cells were exposed to  $0.2 \text{ W cm}^{-2}$  light irradiation for 10 minutes, followed by incubation in fresh medium for 24 and 48 h, respectively. The results suggested that the cRGD-siVEGF-TTD NPs showed obvious cytotoxicity to MDA-MB-231 cells and the viability of MDA-MB-231 cells without light illumination decreased to 61% after 48 h, which was mainly caused by delivered siVEGF though RNA interference. Exposure to light irradiation resulted in a further decrease of the viability of MDA-MB-231 cells to 25% after 48 h. It is noteworthy that the viability of MDA-MB-231 cells treated with cRGD-TTD NPs without surface siVEGF remained 70% after the same PDT treatment while the light irradiation itself did not cause damage to cell viability (Fig. S9, ESI†). These data confirmed the synergistic effect of RNA interference and PDT effect, which could lead to more effective therapeutic outcome. From Fig. 3B, it could also be seen that the viability of MDA-MB-231 cells after cRGD-siVEGF-TTD NP treatment was significantly lower as compared to that of SK-BR-3 and MFC-7 cells under the same experimental conditions, revealing the targeted therapeutic effect of cRGD-siVEGF-TTD NP to integrin-overexpressed cancer cells.

In conclusion, a new multifunctional AIE NP based siRNA vector was successfully developed for combined image-guided PDT and RNAi therapy for targeted cancer cells. The platform shows bright fluorescence and could effectively generate ROS under light irradiation. VEGF siRNA conjugated on the surface of NPs has been successfully transfected to cancer cells to downregulate VEGF mRNA and protein expressions. Cell viability studies showed that the siVEGF-TTD NPs could selectively and efficiently kill the  $\alpha_v\beta_3$  integrin overexpressed cancer cells with the synergistic effect between PDT and RNA interference. In future, AIE photosensitizers with efficient absorption in the long wavelength region will be promising for exploring the potential of such a multifunctional theranostic platform in *in vivo* research.

The authors are grateful to the A\*STAR Joint Council Office and Institute of Materials Research and Engineering of Singapore (13302FG056 and IMRE/13-8P1104), the Singapore National Research Foundation (R-279-000-444-281), the SMART Innovation Grant (R279-000-378-592), the Research Grants Council of Hong Kong (16305015, 16303015 and N\_HKUST640/14), and the University Grants Committee of Hong Kong (AoE/P-03/08) for financial support. K. Li thanks A\*STAR for support *via* A\*STAR International Fellowship.

## Notes and references

- O. Taratula, C. Schumann, T. Duong, K. L. Taylor and O. Taratula, *Nanoscale*, 2015, 7, 3888–3902.
- (a) J. F. Gohy and Y. Zhao, *Chem. Soc. Rev.*, 2013, 42, 7117–7129; (b) D. Wang, B. Fei, L. V. Halig, X. Qin, Z. Hu, H. Xu, Y. A. Wang, Z. Chen, S. Kim, D. M. Shin and Z. Chen, *ACS Nano*, 2014, 8, 6620–6632; (c) X. Liang, X. Li, L. Jing, X. Yue and Z. Dai, *Biomaterials*, 2014, 35, 6379–6388.
- (a) *Photophysics of Aromatic Molecules*, ed. J. B. Birks, Wiley, 1970; (b) *Handbook of Porphyrin Science: with Applications to Chemistry, Physics, Materials Science, Engineering, Biology and Medicine*, ed. K. M. Kadish, K. M. Smith and R. Guilard, World Scientific, 2010; (c) N. Sekkat, H. v. d. Bergh, T. Nyokong and N. Lange, *Molecules*, 2012, 17, 98–144.
- (a) D. Ding, K. Li, B. Liu and B. Z. Tang, *Acc. Chem. Res.*, 2013, 46, 2441–2453; (b) H. Shi, J. Liu, J. Geng, B. Z. Tang and B. Liu, *J. Am. Chem. Soc.*, 2012, 134, 9569–9572; (c) D. Ding, C. C. Goh, G. Feng, Z. Zhao, J. Liu, R. Liu, N. Tomczak, J. Geng, B. Z. Tang, L. G. Ng and B. Liu, *Adv. Mater.*, 2013, 25, 6083–6088; (d) K. Li, W. Qin, D. Ding, N. Tomczak, J. Geng, R. Liu, J. Liu, X. Zhang, H. Liu, B. Liu and B. Z. Tang, *Sci. Rep.*, 2013, 3, 1150; (e) Y. Yuan, R. T. Kwok, B. Z. Tang and B. Liu, *J. Am. Chem. Soc.*, 2014, 136, 2546–2554; (f) Q. Hu, M. Gao, G. Feng and B. Liu, *Angew. Chem., Int. Ed.*, 2014, 53, 14225–14229; (g) K. Li and B. Liu, *Chem. Soc. Rev.*, 2014, 43, 6570–6597.
- Y. N. Hong, J. W. Y. Lam and B. Z. Tang, *Chem. Soc. Rev.*, 2011, 40, 5361–5388.
- (a) G. Feng, Y. Yuan, H. Fang, R. Zhang, B. Xing, G. Zhang, D. Zhang and B. Liu, *Chem. Commun.*, 2015, 51, 12490–12493; (b) Y. Yuan, C. J. Zhang, M. Gao, R. Zhang, B. Z. Tang and B. Liu, *Angew. Chem., Int. Ed.*, 2015, 54, 1780–1786; (c) C. J. Zhang, Q. Hu, G. Feng, R. Zhang, Y. Yuan, X. Lu and B. Liu, *Chem. Sci.*, 2015, 6, 4580–4586.
- S. Y. Park, H. J. Baik, Y. T. Oh, K. T. Oh, Y. S. Youn and E. S. Lee, *Angew. Chem., Int. Ed.*, 2011, 50, 1644–1647.
- (a) D. E. Dolmans, D. Fukumura and R. K. Jain, *Nat. Rev. Cancer*, 2003, 3, 380–387; (b) D. Trachootham, J. Alexandre and P. Huang, *Nat. Rev. Drug Discovery*, 2009, 8, 579–591; (c) C. Xia, Q. Meng, L. Z. Liu, Y. Rojanasakul, X. R. Wang and B. H. Jiang, *Cancer Res.*, 2007, 67, 10823–10830; (d) A. Ferrario, K. von Tiehl, S. Wong, M. Luna and C. J. Gomer, *Cancer Res.*, 2002, 62, 3956–3961.
- (a) H. Y. Wang, W. J. Yi, S. Y. Qin, C. Li, R. X. Zhuo and X. Z. Zhang, *Biomaterials*, 2012, 33, 8685–8694; (b) X. Cai, H. Zhu, H. Dong, Y. Li, J. Su and D. Shi, *Adv. Funct. Mater.*, 2014, 3, 1818–1827.
- J. Gilleron, W. Querbes, A. Zeigerer, A. Borodovsky, G. Marsico, U. Schubert, K. Manygoats, S. Seifert, C. Andree, M. Stöter, H. Epstein-Barash, L. Zhang, V. Kotliansky, K. fitzgerald, E. Fava, M. Bickle, Y. Kalaidzidis, A. Akinc, M. Maier and M. Zerial, *Nat. Biotechnol.*, 2013, 31, 638–646.
- T. Musacchio, O. Vaze, D. D'Souza and V. P. Torchilin, *Bioconjugate Chem.*, 2010, 21, 1530–1536.
- Y. Yuan, G. Feng, W. Qin, B. Z. Tang and B. Liu, *Chem. Commun.*, 2014, 50, 8757–8760.
- R. Mo, T. Jiang, R. DiSanto, W. Tai and Z. Gu, *Nat. Commun.*, 2014, 5, 3364.
- W. Qin, D. Ding, J. Liu, W. Z. Yuan, Y. Hu, B. Liu and B. Z. Tang, *Adv. Funct. Mater.*, 2012, 22, 771–779.
- J. Zhao, Y. Mi and S. S. Feng, *Biomaterials*, 2013, 34, 3411–3421.
- A. P. Castano, T. N. Demidova and M. R. Hamblin, *Photodiagn. Photodyn. Ther.*, 2004, 1, 279–293.
- J. Ge, M. Lan, B. Zhou, W. Liu, L. Guo, H. Wang, Q. Jia, G. Niu, X. Huang, H. Zhou, X. Meng, P. Wang, C. S. Lee, W. Zhang and X. Han, *Nat. Commun.*, 2014, 5, 4596.
- L. Xiao, L. Gu, S. B. Howell and M. J. Sailor, *ACS Nano*, 2011, 5, 3651–3659.
- (a) B. Zhao, J. J. Yin, P. J. Bilski, C. F. Chignell, J. E. Roberts and Y. Y. He, *Toxicol. Appl. Pharmacol.*, 2009, 241, 163–172; (b) N. M. Idris, M. K. Gnanasamandhan, J. Zhang, P. C. Ho, R. Mahendran and Y. Zhang, *Nat. Med.*, 2012, 18, 1580–1585.
- T. Thambi, G. Saravanakumar, J. U. Chu, R. Heo, H. Ko, V. Deepagan, J. H. Kim and J. Park, *Macromol. Res.*, 2013, 21, 100–107.
- F. Zhao, G. Shen, C. Chen, R. Xing, Q. Zou, G. Ma and X. Yan, *Chem. – Eur. J.*, 2014, 20, 6880–6887.
- M. Morini, M. Mottolese, N. Ferrari, F. Ghiorzo, S. Buglioni, R. Mortarini, D. M. Noonan, P. G. Natali and A. Albini, *Int. J. Cancer*, 2000, 87, 336–342.
- (a) Q. Zhan, W. Yue and S. Hu, *Photodiagn. Photodyn. Ther.*, 2011, 8, 314–320; (b) J. Song, Q. Chen and D. Xing, *Exp. Cell Res.*, 2013, 319, 1491–1504; (c) W. H. Chen, R. L. G. Lecaros, Y. C. Tseng, L. Huang and Y. C. Hsu, *Cancer Lett.*, 2015, 359, 65–74.
- R. L. G. Lecaros, L. Huang and Y. C. Hsu, *Proc. Soc. Photo-Opt. Instrum. Eng.*, 2014, 8944, 894405.